



CHALMERS
UNIVERSITY OF TECHNOLOGY

Master-slave carrier recovery for M-QAM multicore fiber transmission

Downloaded from: <https://research.chalmers.se>, 2019-11-13 18:51 UTC

Citation for the original published paper (version of record):

Lundberg, L., Puttnam, B., Luís, R. et al (2019)

Master-slave carrier recovery for M-QAM multicore fiber transmission







Optics Express, 27(16): 22226-22236

<http://dx.doi.org/10.1364/OE.27.022226>

N.B. When citing this work, cite the original published paper.



Master-slave carrier recovery for M-QAM multicore fiber transmission

LARS LUNDBERG,^{1,2}  BENJAMIN J. PUTTNAM,¹  RUBEN S. LUÍS,¹  GEORG RADEMACHER,¹  MAGNUS KARLSSON,^{2,*}  PETER A. ANDREKSON,²  YOSHINARI AWAJI,¹ AND NAOYA WADA¹

¹National Institute of Information and Communications Technology (NICT), 4-2-1 Nukui-kita, Koganei, Tokyo 184-8795, Japan;

²Photonics Laboratory, Department of Microtechnology and Nanoscience (MC2), Chalmers University of Technology, SE-41296 Gothenburg, Sweden

*magnus.karlsson@chalmers.se

Abstract: Master-slave carrier recovery is a digital signal processing technique that uses correlated phase noise in multi-channel receivers to eliminate redundant carrier recovery blocks. In this paper we experimentally investigate the performance of master-slave carrier recovery for multicore fiber transmission in the presence of inter-channel nonlinear interference. Using a triple parallel loop setup we jointly receive three spatial channels in a 7-core fiber for transmission distances of up to 1600 km. We find that an increased launch power causes a moderate penalty on the slave channels. Furthermore, we study the penalty from a non-zero inter-core skew.

© 2019 Optical Society of America under the terms of the [OSA Open Access Publishing Agreement](#)

1. Introduction

Spatial-division multiplexing (SDM) has been widely proposed as a next step in the development of fiber optical communication systems [1]. Combined with wavelength-division multiplexing (WDM) and advanced modulation formats, it has allowed record transmission rates through a single fiber [2,3]. However, to become an attractive step to take, it is not enough to offer only increased capacity, there also needs to be cost benefits. One limiting factor of modern systems is the power consumption and size of transceivers [4]. In this regard, SDM offers several advantages, one of which is the potential for transceiver integration and hardware sharing, e.g. by using the same light source to supply carrier and local oscillator (LO) to many spatial channels. Apart from the size benefits, this also means that the spatial channels experience largely the same laser phase noise [5,6], which enables power consumption savings by eliminating redundant digital signal processing (DSP) blocks through master-slave carrier recovery [7].

Master-slave carrier recovery is one of several kinds of joint carrier recovery methods, which denotes signal processing schemes relying on phase and frequency correlations in multi-channel systems. This includes common polarization multiplexed systems [8], SDM systems in multicore and multimode fiber [5,6] and phase coherent spectral superchannels [9–11]. In addition to reducing DSP complexity, joint carrier recovery can be used to increase tolerance to phase noise [10,12] and to enable cycle slip mitigation [13].

Previous demonstrations of joint carrier recovery in multicore fiber transmission (MCF) have either been limited to a single span and low-order modulation formats [5] or disregarded wavelength division multiplexed (WDM) transmission [12]. This means that they did not consider nonlinear interference from surrounding channels. As inter-channel nonlinear interference will in part manifest itself as phase-noise that can be tracked by the carrier recovery subsystem [14], each spatial channel in an MCF carrying WDM signals will have distinct nonlinear contributions to the phase noise. The impact of this effect on joint carrier recovery is yet to be investigated.

Furthermore, MCFs suffer from small differences in transmission properties between the cores due to imperfections in the manufacturing process. In particular, differences in the effective

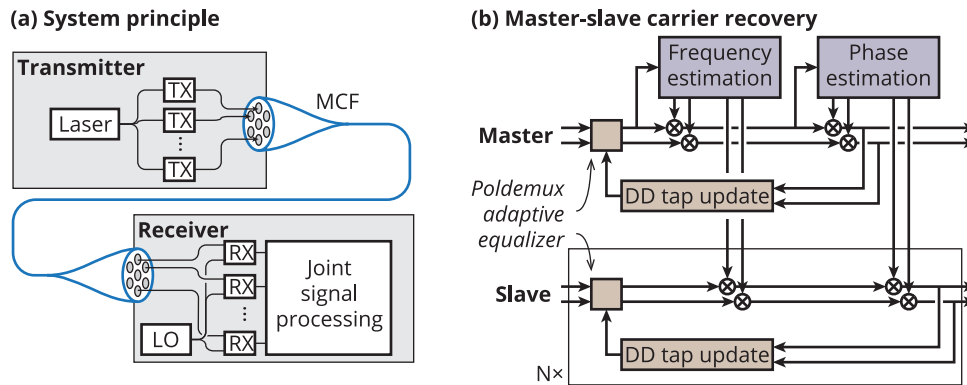


Fig. 1. (a) Principle of a multicore fiber link enabling joint carrier recovery. (b) Master-slave carrier recovery performed inside the update loop of the main adaptive equalizer used for polarization demultiplexing with a decision directed (DD) tap update algorithm. This way, slow differences between the master and slave channels can be tracked by the equalizer. MCF: Multicore fiber.

index of the cores causes a static temporal skew between the spatial channels, which can be as high as several hundreds of ps/km [15]. Although static skew can be compensated by inserting fixed optical delays, such a solution would be unpractical when moving towards SDM systems with fully integrated transceivers and amplifiers. In the previous demonstrations, the inter-core skew was either not considered [5] or compensated for using optical delays [12].

In this paper we study the performance of master-slave carrier recovery in a 7-core fiber for transmission distances of up to 1600 km in a triple parallel recirculating loop experiment. Each core carries 87 channels modulated with 24.5 Gbd polarization multiplexed 16QAM or 64QAM signals. First, we investigate the penalty associated with increased signal launch power with the inter-core time skew fully compensated. We find that an increased launch power is associated with a moderate penalty on the slave channels, leading to a shorter reach. Secondly, we investigate the penalty associated with a non-zero skew by inserting a controlled amount of delay in one of the spatial channels.

2. Master-slave carrier recovery for multicore transmission

Master-slave carrier recovery has the purpose of reducing DSP complexity in multichannel systems with correlated phase-noise. The principle is that the frequency offset and phase noise are estimated from one channel – the master channel – and used for several slave channels. This means that redundant estimation blocks can be eliminated, which reduces power consumption and chip area in the DSP electronics [7]. Any blind carrier recovery algorithm can be used for the master phase-estimation, as long as the estimated phase-noise can be extracted and applied to the slave channels. The performance of the slave channels in terms of linewidth tolerance will then be dictated by the carrier-recovery algorithm used for the master channel.

In MCF transmission systems phase-noise correlation is achieved by sharing the transmitter and receiver light sources between the spatial channels, as illustrated in Fig. 1(a). The phase relation between the spatial channels is then maintained during transmission owing to the stable relation between the transmission properties of the different cores [15]. The fundamental principle is similar to self-homodyne [16] and shared-carrier reception systems [17,18], where one core is dedicated to an unmodulated carrier that acts as a pilot tone. However, in contrast to systems using a pilot tone, joint carrier recovery does not decrease the spectral efficiency.

Similar to self-homodyne systems, master-slave carrier recovery requires the difference in propagation delay (the total accumulated inter-core skew) of the spatial channels to be minimized. A static time difference can be compensated by applying a corresponding opposite time delay. However, it is important to realize that to preserve the phase coherence after detection, the delay compensation needs to be performed in the optical domain. Without optical delay compensation, delays between spatial channels will translate to delayed LO mixing. Then, if an electronic delay is applied to align the phase noise contributions from the carrier, instead the phase noise contribution from the LOs will be misaligned. Therefore electronic delays after detection cannot fully compensate for differences in propagation delay. If the skew is not compensated, the phase-noise compensation of the slave channels will be imperfect and some phase noise will remain on the slave channels. Assuming that the master and slave channels are affected by identical phase noise $\phi(t)$ apart from a time skew T , the remaining phase noise can be written

$$\phi_{\text{slave}}(t) = \phi(t) - \phi(t - T). \quad (1)$$

If the transmitter light source has a Lorentzian linewidth of $\Delta\nu$, $\phi(t)$ is a Wiener process with variance parameter $2\pi\Delta\nu$. Then, the remaining phase noise $\phi_{\text{slave}}(t)$ is a zero-mean Gaussian process with a variance of $2\pi\Delta\nu|T|$ [19,20]. Hence, penalties caused by skew will be higher if a higher-linewidth carrier light source is used. Further analysis of performance penalties due to skew can be found in [20,21].

The specific implementation of master-slave carrier recovery used in this paper is illustrated in Fig. 1(b). All steps of the carrier recovery are performed within the update loop of the main decision-directed (DD) adaptive equalizer used for polarization demultiplexing. This scheme is similar to how DD equalizers are commonly implemented together with independent carrier recovery [22], and was also used together with master-slave carrier recovery in [5]. Since the equalizer uses a DD tap update algorithm, it can track slowly varying remaining phase errors after carrier recovery. This has the added benefit that slow phase differences between the master and the slave that may occur due to vibrations and temperature differences [15] will be at least partly compensated, reducing performance degradation on the slave channels.

To not over-estimate the equalizer's ability to track phase differences between the channels the taps are updated every 64th symbol, which emulates hardware parallelization [23]. Frequency offset estimation is done by finding the peaks in the 4th power spectrum [24], and the phase estimation is performed with a blind phase search (BPS) algorithm [19], with angle interpolation to reduce the number of required test-phases [25].

3. Experiments

To evaluate joint carrier recovery we performed transmission experiments using a triple parallel loop setup. A schematic of the experimental setup is shown in Fig. 2. In the transmitter, a frequency comb [26] was used to produce 87 carriers with a spacing of 25 GHz that were modulated with 24.5-GBd signals. The channels were divided into a test and a loading band. For the test band, 5 comb lines were filtered out and split into even and odd lines, which were modulated with inverted versions of the same data in two dual polarization IQ-modulators, after which they were decorrelated with a few meters of fiber. The center channel of the test band was used as the channel under test, which was set at 1545.32 nm. The modulators were driven by a four-channel arbitrary waveform generator (AWG) operating at 49 GS/s. For the loading channels, 87 lines were modulated in a single polarization IQ-modulator driven with a one-channel AWG equivalent to the test-band AWG. Polarization multiplexing was emulated by splitting the signal into two components. One was delayed before recombining the two parts in orthogonal polarizations. The loading channels were then power-flattened in two cascaded optical processors, the last of which also blocked the channels corresponding to the test band. The signals used were pre-equalized root-raised cosine signals with a roll-off factor of 0.01, using

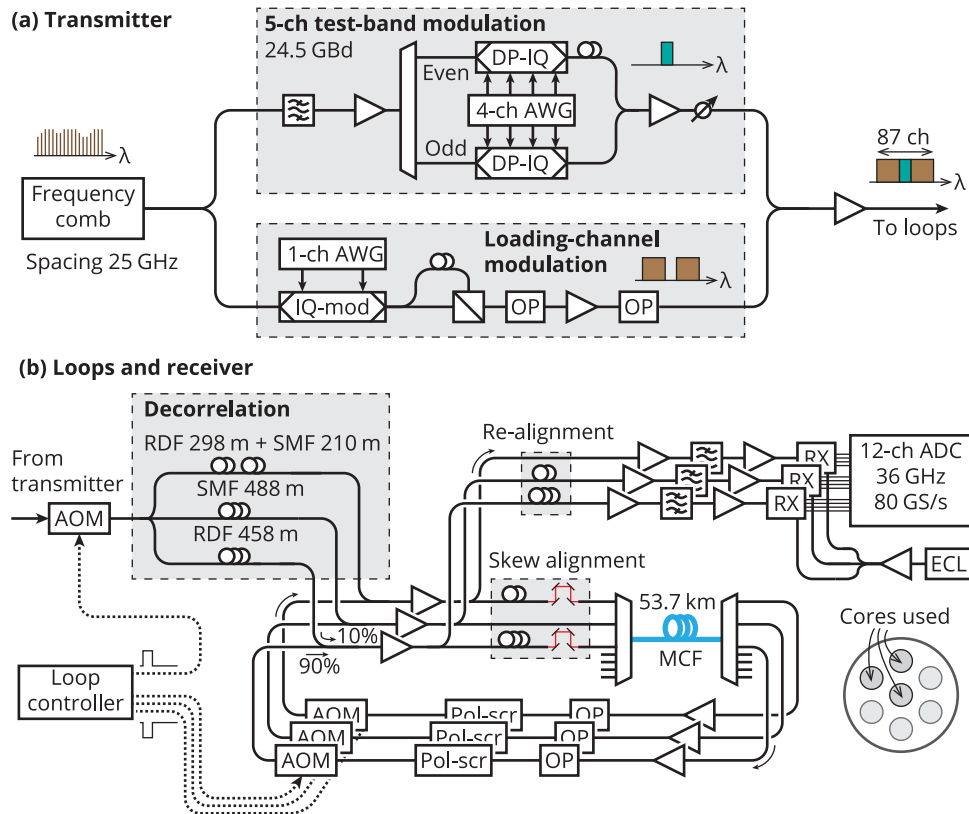


Fig. 2. Schematic of the experimental setup. (a) Wavelength division multiplexing transmitter based on an optical frequency comb. (b) Triple parallel loop setup and three-channel receiver. AWG: arbitrary waveform generator, DP-IQ: Dual polarization in-phase-quadrature modulator, OP: Optical processor, AOM: Acousto-optic modulator, RDF: Reverse-dispersion fiber, SMF: Standard singlemode fiber, RX: Receiver, ADC: Analog-to-digital converter, ECL: External cavity laser, Pol-scr: Polarization scrambler, MCF: Multicore fiber.

either 16 or 64QAM. After modulation and flattening, the loading channels were combined with the test-band, whose power was adjusted to match the level of the loading channels.

For transmission, three parallel recirculating loops in three cores of a 53.7-km 7-core fiber were used. The 7 cores were arranged in a hexagonal structure with a center core, as seen in Fig. 2. The three cores used for transmission were two neighboring outer cores and the center core. Due to equipment constraints, a single acousto-optic modulator (AOM) was used as a shared loading switch, after which the signal was split using a 1-by-3 coupler and decorrelated. The purpose of the decorrelation was twofold: Firstly, the three signals were delayed with respect to each other to avoid correlated inter-core crosstalk. Secondly, the decorrelation fibers had different amounts of dispersion to decorrelate the surrounding WDM-channels differently with respect to the channel under test to reduce the correlation between nonlinear interference within different cores. However, due to the fact that the split by necessity had to be after the load AOM, the amount of decorrelation possible to apply was limited to avoid loop timing issues and degradation of the optical signal-to-noise ratio (OSNR).

After decorrelation, the signals were coupled into the loops using 10-dB couplers to minimize the loop losses. Within each loop, the signals were amplified using erbium-doped fiber amplifiers

(EDFAs) once before being input into the MCF. The launch power was varied by changing the output power of the launch EDFAs. After transmission through the fiber, the signals were amplified again, followed by gain flattening and loop-synchronous polarization scrambling. The signal used in the receiver path was taken from the 10-dB couplers after the launch EDFAs.

The three loops were path-length matched using patch-cords and variable delay lines. This compensated for both the length difference of the components used in the loop and the time-skew of the cores. To study the effect of time skew, a controlled delay was inserted into one of the loops instead.

In the receiver, path-length matching was applied to compensate for the decorrelation of the signals, after which the signals were amplified and filtered before detection in three standard dual-polarization coherent receivers. Light from a less than 100-kHz linewidth external cavity laser (ECL) was amplified and split to be used as a common local oscillator (LO). The signals were then sampled at 80 GS/s using a 12-channel real-time oscilloscope with a bandwidth of 36 GHz.

The phase-noise properties of the transmitter comb are characterized in [27]. The 1545.32-nm comb-line used for the test-channel can be described by a linewidth of roughly 20 kHz, but it should be noted that since the frequency noise of the comb-line is not spectrally flat, the phase-noise properties are not fully described by a Lorentzian linewidth. The LO laser had a linewidth specified to be below 100 kHz, typically 25 kHz.

Digital signal processing (DSP) was performed offline. It consisted of orthonormalization, resampling to two samples per symbol, dispersion compensation and matched filtering followed by adaptive equalization and a second orthonormalization step to compensate for modulator bias imperfections. The adaptive equalizer had 33 half-symbol-spaced taps that were pre-converged using the constant modulus algorithm (CMA). The equalizer was then switched to decision directed (DD) mode with carrier recovery in the update loop according to the description in Section 2. The step size of the equalizer was 10^{-3} during CMA pre-convergence and 10^{-4} in DD mode. Furthermore, the frequency offset estimation was performed over 500000 symbols, the BPS blocklength was 128 symbols, and the number of test phases used was 8 and 16 for 16QAM and 64QAM respectively. The low number of test phases was possible due to the angle interpolation in the BPS algorithm used [25].

4. Results and discussion

In this section we compare performance using master-slave carrier recovery with the performance of standard independent carrier recovery. In this way we can study the penalty associated with master-slave carrier recovery as a function of transmission distance, launch power and inter-core time skew. Since only three cores arranged in a triangle were loaded with data, the cores suffered from the same crosstalk. This means that performance differences due to different crosstalk levels are not studied, but we note that additional crosstalk on some cores possible in some fiber designs could have an impact on master-slave carrier recovery, similar to self-homodyne detection [16]. The performance is characterized using the generalized mutual information (GMI) which is the maximum achievable data throughput accounting for the overhead of an ideal forward error correcting code using a bit-wise receiver [28]. The GMI is calculated based on more than 3 million bits using the method described in [29].

4.1. Impact of launch power

The master-slave penalty was evaluated for total launch powers between 11 dBm and 19 dBm per core, corresponding to -8 dBm and 0 dBm per channel. The same launch power was used in all three cores. Figure 3 and 4 shows the GMI as a function of transmission distance and launch power for one of the outer cores and the center core, for 16QAM and 64QAM respectively. For each core, the performance of independent processing is compared to master-slave processing

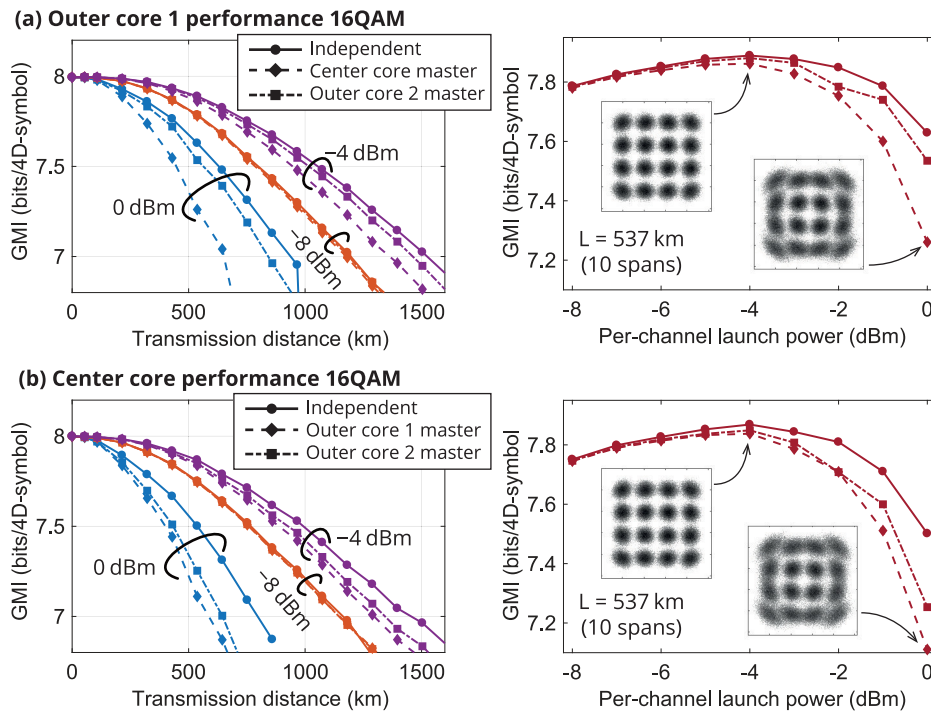


Fig. 3. Experimental results for 16QAM. Comparison of the GMI using either standard independent carrier recovery or master-slave carrier recovery. The master phase is taken from either of the remaining two cores. (a) Outer-core performance. (b) Center-core performance. The insets show constellation diagrams for master-slave carrier recovery at optimal and at the highest launch power.

using the two other cores respectively as master. The performance of the outer cores was similar, so only one is plotted. For linear transmission, the penalty for master-slave processing is negligible. However, master-slave processing causes a penalty that increases with launch power and transmission distance. For the outer cores, the nonlinear penalty is lower when the other outer core is used as master. This is likely due to a combination of experimental limitations and differences in transmission properties between the center core and the outer cores. The limitations in the signal decorrelation likely causes the nonlinear contribution to the phase noise to still be partly correlated. However, as the center core has a different dispersion parameter, the nonlinear phase noise in that core will be further decorrelated during transmission, and cause a higher penalty when used in a master-slave scheme. In addition, since dynamic gain flattening was performed inside each loop, slight variations in loss between components in different loops would have resulted in small launch power variation between cores and as a function of distance. Some variation in the loss of fan-in-fan-out at the input to the MCF may also cause errors in the recorded launch power. As different launch powers cause the nonlinear phase noise contributions to differ between the cores, this is likely contributing to the differences in nonlinear penalty of the cores.

To investigate the effect of random data carried on the interfering channels on the nonlinear penalty, we also performed split-step simulations. The fiber and signal parameters were set to match the experiments, with the exception of the data patterns on the channels, which were random and independent in the simulation. Furthermore, the number of channels was reduced to 19 to reduce simulation time, and only the single-polarization case was studied. Multicore

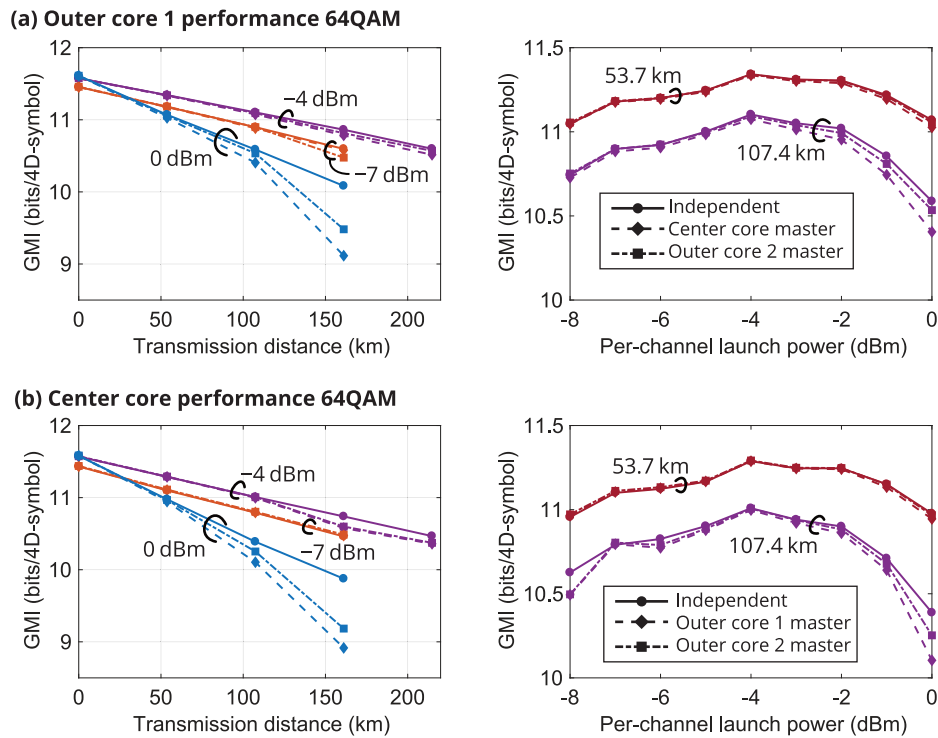


Fig. 4. Experimental results for 64QAM. Comparison of the GMI using either standard independent carrier recovery or master-slave carrier recovery. The master phase is taken from either of the remaining two cores. (a) Outer-core performance. (b) Center-core performance.

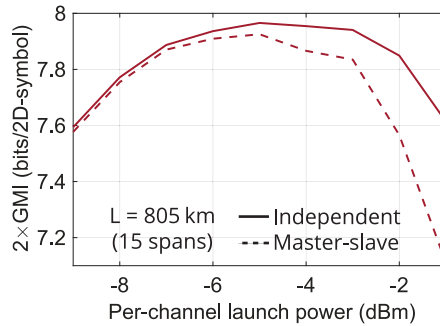
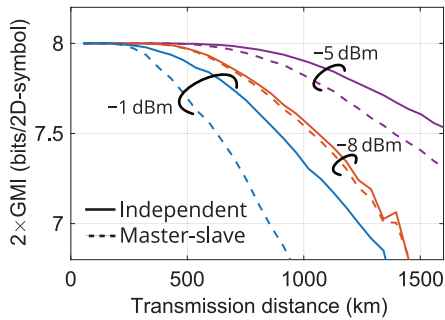
transmission was simulated as two separate simulations with different data patterns and different ASE noise realizations, but with the same phase noise realizations. Phase noise was modelled as a Wiener process corresponding to a linewidth of 50 kHz on the carrier and LO. The transmitter and receiver were assumed to be ideal, but a loss of 18 dB was added after each span to simulate loop transmission. The simulation results are shown in Fig. 5. The general behaviour of the slave penalty is similar to the outer-center core combination in our experiments, indicating that the outer-outer core combination likely underestimates the slave penalty.

We note that the issue of realistic loading in WDM system experiments with limited equipment is an ongoing topic of discussion in the fiber optical communication research community [30,31]. The challenges are further increased when scaling into the spatial dimensions. In our experiments, two counteracting effects occurred due to equipment limitations. The first one was that the decorrelation of the WDM channels had to be limited, which lead to some remaining correlation of the nonlinear contributions to the phase noise. The second one was that the same data was used on all 82 loading channels, which exaggerates the nonlinear phase noise. In the end, the nonlinear penalty will depend on the statistics of the nonlinear phase noise, which will depend on many factors such as baud-rate, channel spacing, modulation format and span length.

4.2. Inter-core skew

Inter-core temporal skew was experimentally investigated by inserting different lengths of patch-cords into the loop of outer core 1. The launch power used was -4 dBm per channel. This way a length-dependent skew was emulated, as the path-length difference is multiplied by the number of roundtrips. Skew values up to 650 ps/km was tested for 16QAM and up to 200 ps/km for

(a) Simulation results 16QAM



(b) Simulation results 64QAM

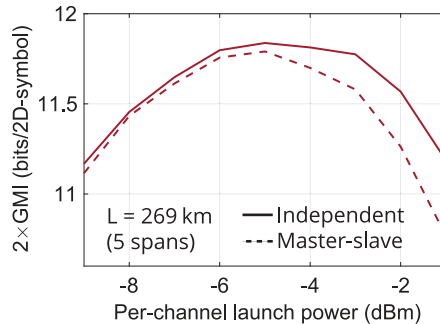
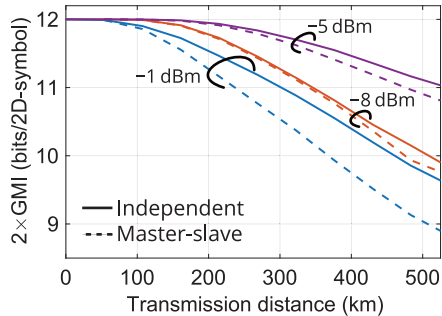


Fig. 5. Split-step simulation results with random and independent data on the interfering channels. The single-polarization GMI-values have been doubled to make comparisons with experimental results easier. (a) 16QAM (b) 64QAM.

64QAM. This should be compared to the natural inter-core skew in the MCF span used that ranged between 2 and 500 ps/km for different core combinations [15]. The GMI as a function of transmission distance for different amounts of skew is shown in Fig. 6. It is evident that time-skew heavily penalises the slave channels, as the reach is severely limited for all but the smallest skew values. Nevertheless, for short transmission distances, some amount of skew can be accepted. Furthermore, the penalties will depend on the linewidth of the transmitter light source, where a higher linewidth causes higher penalties [20,21]. In this regard, the comb-line used in the above measurements behaved like an ECL-laser with less than 100-kHz linewidth, similar to the LO laser.

The investigated cases represent a worst-case scenario where the same skew accumulates span after span. In a multispan transmission link, the average skew would be smaller. Furthermore, the presence of partly correlated nonlinear phase noise in our measurements likely gives a higher penalty for the cases with skew. Nevertheless, our results highlight the need for skew engineering in systems with joint carrier recovery. This could either be by fiber design, by periodic skew compensation, or by matching fiber spans with opposite skew. The requirements for joint carrier recovery are similar to other joint-processing schemes such as MIMO-processing for crosstalk mitigation [32].

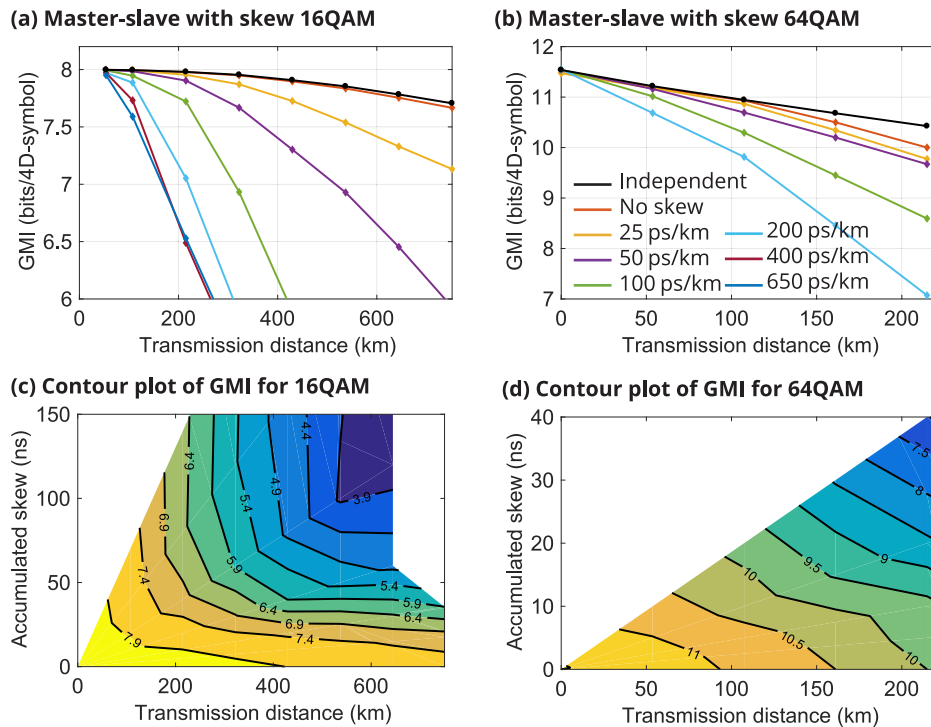


Fig. 6. Experimental results for transmission with intercore skew. Performance of the center core with a launch power of -4 dBm per channel is shown. (a) and (b) Comparison of the GMI as a function of transmission distance for different amounts of inter-core skew for 16QAM and 64QAM respectively. (c) and (d) Contour plot of the GMI as a function of transmission distance and total accumulated skew for 16QAM and 64QAM respectively. White areas represent combinations where no measurements were made.

5. Conclusions

We have investigated master-slave carrier recovery in multicore WDM transmission, via a triple parallel recirculating loop experiment. Our experiments show that for linear transmission, the penalty compared to standard, independent carrier recovery is negligible, but for higher launch powers a transmission-distance dependent, moderate penalty causes a decreased reach for the slave channels. Through simulations we study the impact of the data-pattern on the interfering channels on the penalty. Our results show that joint-core carrier recovery is compatible with dense WDM, and illustrates the potential for combining joint-core and joint-wavelength schemes in frequency comb based hybrid superchannels. Although this study considers square-QAM formats, the conclusions are valid for any modulation formats that are compatible with blind carrier recovery, e.g. geometrically or probabilistically shaped formats.

Furthermore, we have investigated the effect of a static inter-core time skew. We find that skew in the order of magnitude that occurs naturally in MCF may cause penalties for longer transmission distances if left uncompensated. In a field-installed link, master-slave carrier-recovery would therefore require fiber with lower inter-core skew or skew compensation.

Finally, it should be noted that we used a weakly-coupled MCF in this paper and did not consider different cross-talk levels. Further studies are needed to investigate the compatibility of joint-carrier recovery with SDM systems with higher crosstalk levels.

Funding

Knut och Alice Wallenbergs Stiftelse.

Acknowledgments

The authors thank Benjamin Foo for providing the code for the split-step simulations, and Mikael Mazur for fruitful discussions.

References

1. D. J. Richardson, J. M. Fini, and L. E. Nelson, "Space-division multiplexing in optical fibres," *Nat. Photonics* **7**(5), 354–362 (2013).
2. D. Soma, Y. Wakayama, S. Beppu, S. Sumita, T. Tsuritani, T. Hayashi, T. Nagashima, M. Suzuki, H. Takahashi, K. Igarashi, I. Morita, and M. Suzuki, "10.16 peta-bit/s dense SDM/WDM transmission over low-DMD 6-mode 19-core fibre across C+L band," in *European Conference on Optical Communication (ECOC)*, (2017).
3. G. Rademacher, R. S. Luís, B. J. Puttnam, T. A. Eriksson, E. Agrell, R. Maruyama, K. Aikawa, H. Furukawa, Y. Awaji, and N. Wada, "159 Tbit/s C+L band transmission over 1045 km 3-mode graded-index few-mode fiber," in *Optical Fiber Communication Conference (OFC)*, (2018), p. Th4C.4.
4. J. C. Geyer, C. Rasmussen, B. Shah, T. Nielsen, and M. Givehchi, "Power efficient coherent transceivers," in *European Conference on Optical Communication (ECOC)*, (2016), pp. 109–111.
5. M. D. Feuer, L. E. Nelson, X. Zhou, S. L. Woodward, R. Isaac, B. Zhu, T. F. Taunay, M. Fishteyn, J. M. Fini, and M. F. Yan, "Joint digital signal processing receivers for spatial superchannels," *IEEE Photonics Technol. Lett.* **24**(21), 1957–1960 (2012).
6. R. G. H. Van Uden, C. M. Okonkwo, H. Chen, H. De Waardt, and A. M. J. Koonen, "28-GBd 32QAM FMF transmission with low complexity phase estimators and single DPMLL," *IEEE Photonics Technol. Lett.* **26**(8), 765–768 (2014).
7. L. Lundberg, E. Börjeson, C. Fougstedt, M. Mazur, M. Karlsson, P. A. Andrekson, and P. Larsson-Edefors, "Power consumption savings through joint carrier recovery for spectral and spatial superchannels," in *European Conference on Optical Communication (ECOC)*, (2018).
8. R. Noé, "Phase noise-tolerant synchronous QPSK/BPSK baseband-type intradyne receiver concept with feedforward carrier recovery," *J. Lightwave Technol.* **23**(2), 802–808 (2005).
9. L. Lundberg, M. Karlsson, A. Lorences-Riesgo, M. Mazur, V. Torres-Company, J. Schröder, and P. A. Andrekson, "Frequency comb-based WDM transmission systems enabling joint signal processing," *Appl. Sci.* **8**(5), 718 (2018).
10. D. V. Souto, B.-E. Olsson, C. Larsson, and D. A. A. Mello, "Joint-polarization and joint-subchannel carrier phase estimation for 16-QAM optical systems," *J. Lightwave Technol.* **30**(20), 3185–3191 (2012).
11. D. S. Millar, R. Maher, D. Lavery, T. Koike-Akino, M. Pajovic, A. Alvarado, M. Paskov, K. Kojima, K. Parsons, B. C. Thomsen, S. J. Savory, and P. Bayvel, "Design of a 1 Tb/s superchannel coherent receiver," *J. Lightwave Technol.* **34**(6), 1453–1463 (2016).
12. A. F. Alfredsson, E. Agrell, H. Wymeersch, B. J. Puttnam, G. Rademacher, R. S. Luis, and M. Karlsson, "Pilot-aided joint-channel carrier-phase estimation in space-division multiplexed multicore fiber transmission," *J. Lightwave Technol.* **37**(4), 1133–1142 (2019).
13. M. Qiu, Q. Zhuge, Y. Gao, W. Wang, F. Zhang, and D. Plant, "Cycle slip mitigation with joint carrier phase recovery in coherent subcarrier multiplexing systems," in *Optical Fiber Communication Conference (OFC)*, (2016) p. Tu3K.2.
14. R. Dar, M. Feder, A. Mecozzi, and M. Shtaf, "Properties of nonlinear noise in long, dispersion-uncompensated fiber links," *Opt. Express* **21**(22), 25685–25699 (2013).
15. B. J. Puttnam, G. Rademacher, R. S. Luís, J. Sakaguchi, Y. Awaji, and N. Wada, "Inter-core skew measurements in temperature controlled multi-core fiber," in *Optical Fiber Communication Conference (OFC)*, (2018) p. Tu3B.3.
16. B. J. Puttnam, J. Sakaguchi, J. M. D. Mendinueta, W. Klaus, Y. Awaji, N. Wada, A. Kanno, and T. Kawanishi, "Investigating self-homodyne coherent detection in a 19 channel space-division-multiplexed transmission link," *Opt. Express* **21**(2), 1561–1566 (2013).
17. E. Le Taillandier de Gabory, M. Arikawa, Y. Hashimoto, T. Ito, and K. Fukuchi, "A shared carrier reception and processing scheme for compensating frequency offset and phase noise of space-division multiplexed signals over multicore fibers," in *Optical Fiber Communication Conference/National Fiber Optic Engineers Conference*, (2013), p. OM2C.2.
18. R. S. Luís, B. J. Puttnam, G. Rademacher, Y. Awaji, and N. Wada, "PDM-128-QAM transmission using shared carrier reception in a 7-core multi-core fiber," in *Asia Communications and Photonics Conference (ACP)*, (2017), p. M1B.6.
19. T. Pfau, S. Hoffmann, and R. Noé, "Hardware-efficient coherent digital receiver concept with feedforward carrier recovery for M-QAM constellations," *J. Lightwave Technol.* **27**(8), 989–999 (2009).
20. R. S. Luis, B. J. Puttnam, J. M. Delgado Mendinueta, Y. Awaji, and N. Wada, "Impact of spatial channel skew on the performance of spatial-division multiplexed self-homodyne transmission systems," in *International Conference on Photonics in Switching (PS)*, (2015), pp. 37–39.

21. R. S. Luis, B. J. Puttnam, Y. Awaji, and N. Wada, "OSNR penalties for non-zero skew in space-division multiplexed transmission link with self-homodyne detection," in *Asia Communications and Photonics Conference (APC)*, (2015), p. ASu5D.5.
22. M. S. Faruk and S. J. Savory, "Digital signal processing for coherent transceivers employing multilevel formats," *J. Lightwave Technol.* **35**(5), 1125–1141 (2017).
23. C. Fougstedt, P. Johannisson, L. Svensson, and P. Larsson-Edefors, "Dynamic equalizer power dissipation optimization," in *Optical Fiber Communication Conference (OFC)*, (2016), p. W4A.2.
24. S. J. Savory, "Digital coherent optical receivers: Algorithms and subsystems," *IEEE J. Sel. Top. Quantum Electron.* **16**(5), 1164–1179 (2010).
25. H. Sun, K.-T. Wu, S. Thomson, and Y. Wu, "Novel 16QAM carrier recovery based on blind phase search," in *European Conference on Optical Communication (ECOC)*, (2014).
26. B. J. Puttnam, R. S. Luis, W. Klaus, J. Sakaguchi, J.-M. Delgado Mendiñeta, Y. Awaji, N. Wada, Y. Tamura, T. Hayashi, M. Hirano, and J. Marcianti, "2.15 Pb/s transmission using a 22 core homogeneous single-mode multi-core fiber and wideband optical comb," in *European Conference on Optical Communication (ECOC)*, (2015).
27. J. Sakaguchi, Y. Awaji, and N. Wada, "Optimal pilot-tone-aided multi-core fiber transmission using a wideband comb transmitter," *IEEE Photonics Technol. Lett.* **29**(15), 1245–1248 (2017).
28. A. Alvarado, E. Agrell, D. Lavery, R. Maher, and P. Bayvel, "Replacing the soft-decision FEC limit paradigm in the design of optical communication systems," *J. Lightwave Technol.* **34**(2), 707–721 (2016).
29. T. Fehenberger, Calculate generalized mutual information, <https://www.fehenberger.de/code/calcGMI.m>. Accessed 2018-08-06.
30. L. B. Du and A. J. Lowery, "The validity of "Odd and Even" channels for testing all-optical OFDM and Nyquist WDM long-haul fiber systems," *Opt. Express* **20**(26), B445–B451 (2012).
31. D. J. Elson, G. Saavedra, K. Shi, D. Semrau, L. Galdino, R. Killely, B. C. Thomsen, and P. Bayvel, "Investigation of bandwidth loading in optical fibre transmission using amplified spontaneous emission noise," *Opt. Express* **25**(16), 19529–19537 (2017).
32. R. S. Luís, G. Rademacher, B. J. Puttnam, Y. Awaji, and N. Wada, "Long distance crosstalk-supported transmission using homogeneous multicore fibers and SDM-MIMO demultiplexing," *Opt. Express* **26**(18), 24044–24053 (2018).